Article

Direct Nonadiabatic Simulations of the Photoinduced Charge Transfer Dynamics

Published as part of The Journal of Physical Chemistry virtual special issue "Josef Michl Festschrift".

Sharma S. R. K. C. Yamijala* and Pengfei Huo*

Read Online

ACCESS | 📊 Metrics & More | 📰 Article Recommendations | 🆂🆂 Supporting Information

ABSTRACT: We apply direct nonadiabatic dynamics simulations to investigate photoinduced charge transfer reactions. Our approach is based on the mixed quantum-classical fewest switches surface hopping (FSSH) method that treats the transferring electron through time-dependent density functional theory and the nuclei classically. The photoinduced excited state is modeled as a transferring single-electron that initially occupies the LUMO of the donor molecule/moiety. This single-particle electronic wave function is then propagated quantum mechanically by solving the time-dependent Schrödinger equation in the basis of the instantaneous molecular orbitals (MOs) of the entire system. The nonadiabatic transitions among electronic states are modeled using the FSSH approach within the classical-path approximation. We apply this approach to simulate the photoinduced charge transfer dynamics in a few well-characterized molecular systems. Our results are in excellent agreement with both the experimental measurements and high-level (yet expensive) theoretical results.
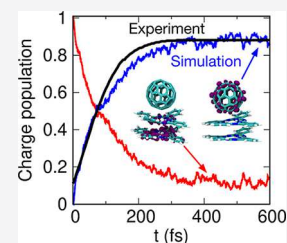
INTRODUCTION

Charge transfer (CT) is a ubiquitous phenomenon that occurs in several chemical reactions, and it plays a fundamental role in many chemical processes.[1−4] Powering chemical reactions through light-driven processes, rather than through relatively brute-force thermally activated processes, would be transformative for society. Photoinduced charge transfer (PICT) across the interface between molecules is crucial for determining the reactivity and efficiency of a photochemical system.

PICT is one of the central reactions that drives solar energy conversion in natural photosynthesis, where the charge-separated state is achieved through multiphoton absorption and involves multiple energy-conversion steps.[5−7] Like the natural process, there are many artificial systems in which the photoinduced charge transfer plays a crucial role.[8−15] Examples include PICT in dye-sensitized solar cells,[8−11,15−17] ultrafast charge-transfer in organic photovoltaic systems,[12−14,18−25] photocatalytic electron/hole transfer in "colloidal quantum dot-organic molecule complex" interfaces,[26−28] and photoinduced proton-coupled electron transfer.[29−31] Understanding the detailed charge transfer dynamics will provide valuable mechanistic insights and design principles for next-generation photocatalytic devices and profoundly impact energy production and catalysis.

The PICT process is often an intrinsic nonadiabatic process, where the transitions among adiabatic electronic states occur through the coupling between electronic and nuclear degrees of freedom (DOF). Accurately and efficiently simulating the nonadiabatic charge transfer dynamics in large-scale systems remains challenging despite encouraging recent progress.[32] This work presents a simple and accurate approach to investigate the

PICT dynamics in model organic molecular systems using on-the-fly simulations.

Our approach uses the fewest switches surface hopping algorithm[32,33] to capture the influence of nuclear vibrations on the electronic nonadiabatic transitions, and the single-particle time-dependent Kohn−Sham (TDKS) approach[8,34,35] to describe the quantum mechanical state of the transferring electron. With this approach, we investigate the nonadiabatic PICT dynamics in the phthalocyanine dimer/fullerene system[12,18,36] and the carotenoid−porphyrin−C_{60} (CPC) triad system,[13,19,22,23,37−39] which are model systems for understanding the CT dynamics in organic photovoltaics. Our results are in excellent agreement with both experimental measurements and high-level (yet expensive) theoretical calculations.

THEORETICAL APPROACH

Our approach to obtain the photoinduced charge-transfer dynamics is based on approximately solving the time-dependent Schrödinger equation (TDSE). Specifically, it is based on the mixed quantum-classical fewest switches surface hopping (FSSH) method that treats the transferring electron through the time-dependent density functional theory, and nuclei classically.
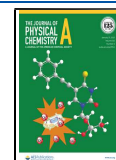
The total Hamiltonian of a system can be expressed as

$$\hat{H} = \hat{T} + \hat{H}_{el} \tag{1}$$

where $\hat{T}$ represents the nuclear kinetic energy operator and $\hat{H}_{el}$ is the electronic Hamiltonian operator. The *adiabatic* electronic ground state $\Phi_0(\mathbf{R})$, which is the eigenstate of $\hat{H}_{el}$, as well as the adiabatic energy $E_0(\mathbf{R})$, are obtained by solving the following time-independent Schrödinger equation (TISE)

$$\hat{H}_{el}|\Phi_0(\mathbf{R})\rangle = E_0(\mathbf{R})|\Phi_0(\mathbf{R})\rangle \tag{2}$$

Among various approaches to solve the above electronic TISE, the Kohn−Sham (KS) density functional theory (DFT) is one of the widely used approaches due to its numerical efficiency. In KS-DFT, the single-particle KS equation is given as

$$\hat{h}_{KS}|\phi_i(\mathbf{R})\rangle = \epsilon_i(\mathbf{R})|\phi_i(\mathbf{R})\rangle \tag{3}$$

where $\hat{h}_{KS}$ is the single-particle KS operator, and $\epsilon_i(\mathbf{R})$ is the energy of the ith molecular-orbital $|\phi_i(\mathbf{R})\rangle$. These molecular orbitals are used to construct the ground state (GS) density,[40] which can be used to compute the ground state energy.

Since solving the TDSE of the total Hamiltonian $\hat{H}$ in eq 1 is a challenging task, in this work, we adapt a set of well-defined and widely tested approximations.[8,10,41].

First, we ignore the influence of electronic excitations on the motion of the nuclei, i.e., the nuclear motion is entirely governed by the ground-state potential energy surface, $E_0(\mathbf{R}(t))$, through the classical equations of motion, given by

$$-\nabla_{\mathbf{R}} E_0(\mathbf{R}) = \mathbf{M}\ddot{\mathbf{R}} \tag{4}$$

The above approximation, known as the classical path approximation (CPA)[41] or the neglect of back-reaction (NBR).,[42] has been extensively tested[41–45] and is proven to provide reasonable results for photoinduced charge transfer dynamics.

Second, we assumed that the photoinduced electron transfer dynamics can be well-described with a single-particle wave function instead of the many-electron wave function. This approximation allows one to use the single-particle version of the time-dependent Kohn−Sham (TDKS) approximation,[32,34,35,46] where the time-dependent *single-particle* excited state $|\Psi(\mathbf{R}(t))\rangle$ can be represented as a linear combination of the ground state KS orbitals[10,11] as

$$|\Psi(\mathbf{R}(t))\rangle = \sum_i c_i(t)|\phi_i(\mathbf{R}(t))\rangle \tag{5}$$

where $\{c_i(t)\}$ are the time-dependent expansion coefficients. The single-particle approximation of the TDKS equation has shown to accurately describe the charge-transfer dynamics[8,10,37,47,48] and excitation energy transfer process.[49] It has been extensively tested against more accurate linear-response (LR)-TDDFT calculations.[35] Note that our eventual goal for this approach is to investigate mesoscopic systems (such as bulk heterojunctions) that contain up to $10^3–10^4$ atoms. For these systems, calculating the excited states through LR-TDDFT are extremely expensive and beyond the practically available computational resources, even with the DFTB approximation.[50] The TDKS approach, on the other hand, has proven to be as accurate as (LR)-TDDFT calculations[35] for a variety of systems, with the numerical cost comparable to a ground state KS calculations. Hence, we choose TDKS in this study.

Within the single-particle TDKS approximation, $|\Psi(\mathbf{R}(t))\rangle$ satisfies the following equation[46]

$$i\hbar\frac{\partial}{\partial t}|\Psi(\mathbf{R}(t))\rangle = \hat{h}_{KS}(\mathbf{R}(t))|\Psi(\mathbf{R}(t))\rangle \tag{6}$$

Plugging eq 5 into eq 6, and multiplying the resulting expression with $\langle\phi_j(t)|$ gives us the following differential equation for the time-dependent expansion coefficients

$$\dot{c}_j(t) = -\frac{i}{\hbar}c_j(t)\epsilon_j(\mathbf{R}(t)) - \sum_i c_i(t)\langle\phi_j(t)|\frac{\partial}{\partial t}\phi_i(t)\rangle \tag{7}$$

where we used shorthand notation $|\phi_i(t)\rangle \equiv |\phi_i(\mathbf{R}(t))\rangle$. The nonadiabatic couplings $\langle\phi_j|\frac{\partial}{\partial t}\phi_i\rangle$ are responsible for electronic transitions among the single-particle adiabatic states. They are related to the derivative coupling vectors through $\langle\phi_j(\mathbf{R}(t))|\frac{\partial}{\partial t}\phi_i(\mathbf{R}(t))\rangle = \langle\phi_j(\mathbf{R}(t))|\nabla|\phi_i(\mathbf{R}(t))\rangle\dot{\mathbf{R}}$.

Third, we adapt the fewest-switches surface hopping (FSSH) algorithm within the CPA approximation[41,45] to describe the electronic nonadiabatic transitions induced by the motion of the nuclei. Solving eq 7 provides $\{c_j(t)\}$, and substituting them in eq 5 gives the time-dependent single-particle electronic wave function, from which one can construct the time-dependent charge transfer density.[10,11] However, due to the lack of microscopic feedback from the electronic subsystem to the nuclear subsystem, directly using the above $c_j(t)$ leads to an incorrect population dynamics[51] that corresponds to an infinite temperature of the electronic subsystem, leading to the artificial equal population among all single-particle electronic states,[51] which is demonstrated in the Supporting Information. To alleviate this problem, and to accurately describe the non-adiabatic transitions among single-particle electronic states, we adapt the fewest-switches surface hopping (FSSH) algorithm within the CPA approximation.[41,45]

During CPA-FSSH dynamics,[41,45] an instantaneous active state is assigned to the system, and the probability of switching from the current state $|\phi_i(\mathbf{R}(t))\rangle$ to any other state $|\phi_j(\mathbf{R}(t))\rangle$ during the time-step $t \in [t, t + \delta]$ is given by[41,45]

$$\tilde{g}_{ij}(t) = -\frac{2\text{Re}\left[c_i^*(t)c_j(t)\langle\phi_j(t)|\frac{\partial}{\partial t}\phi_i(t)\rangle\right]}{c_i^*(t)c_i(t)}\delta t \tag{8}$$

where $\rho_{ij}(t) = c_i^*(t)c_j(t)$ are the adiabatic electronic density matrix elements. In the original FSSH formalism,[33] nuclear velocities are rescaled to conserve the total energy after switching the active states. Within the CPA[9,41] where the back-reaction on the nuclei is neglected, the transition probabilities are rescaled as follows

$$g_{ij}(t) = \max[\tilde{g}_{ij}(t)b_{ij}(t), 0] \tag{9}$$

where $b_{ij}(t) = e^{-(\epsilon_j-\epsilon_i)/k_B T}$ for $\epsilon_j > \epsilon_i$, and $b_{ij}(t) = 1$ for $\epsilon_j \leq \epsilon_i$, $\epsilon_i(\mathbf{R}(t))$ and $\epsilon_j(\mathbf{R}(t))$ are the orbital energies obtained by solving eq 3 with the nuclear configuration $\mathbf{R}(t)$, k_B is the Boltzmann constant, and T is the temperature of the system, which is assumed to be constant during the nonadiabatic dynamics.

A switch from state $|\phi_i(\mathbf{R})\rangle$ to state $|\phi_j(\mathbf{R})\rangle$ takes place when

$$\sum_{k=1}^{k=j-1} g_{ik} < \xi \leq \sum_{k=1}^{k=j} g_{ik} \tag{10}$$

where ξ is a uniform random number between 0 and 1. An ensemble of nuclear trajectories are generated by propagating the nuclei with eq 4, whereas one or more CPA-FSSH

trajectories are generated on top of $R(t)$ by solving eq 7 to obtain the time-dependent electronic expansion coefficients, and then active state is determined based on eq 10. The above procedure is essentially the same as those described in ref 34, apart from a few technical differences. First, we use an accurate charge population estimator (eq 14) as well as the reduced density matrix population estimator (eq 11). To the best of our knowledge, this is the first time that both are used in direct charge transfer CPA-FSSH simulations. Second, we implement the CPA-FSSH approach directly within the DFTB+ software package. For this reason, we do not have to store any elements (such as eigenvalues, eigenvectors, derivative couplings, etc.), which significantly speed up the simulations of large size systems (e.g., thousands of atoms).

We note that FSSH could potentially create an artificial electronic coherence, and a decoherence correction is employed in such circumstances.[33,52] Also, many decoherence approaches are already available for CPA-FSSH.[32,41,43,53] In this work, we choose not to use any decoherence correction because CPA-FSSH already provided an accurate charge transfer dynamics compared to experiments. We compute the adiabatic reduced density matrix as

$$\bar{\rho}_{ij}(t) = \langle \rho_{ij}(t) \rangle \tag{11}$$

where $\langle \cdots \rangle$ represents the ensemble average over the CPA-FSSH trajectories. The estimator $\rho_{ij}(t)$ is expressed as follows[54]

$$\rho_{ii}(t) = \langle \phi_i(R(t)) | \phi_\alpha(R(t)) \rangle = \delta_{i\alpha} \tag{12}$$

$$\rho_{ij}(t) = c_i^*(t) c_j(t) \text{ (for } i \neq j) \tag{13}$$

where, $|\phi_\alpha(\mathbf{R}(t))\rangle$ is the active state at time t along a nuclear trajectory $\mathbf{R}(t)$, and $c_j(t)$ are the corresponding expansion coefficients. The diagonal matrix elements $\rho_{ii}(t)$ are chosen based on the active state $|\phi_\alpha(R(t))\rangle$. Thus, along a specific nuclear trajectory $R(t)$, the instantaneous population at time t is considered to be 1 for the active state $|\phi_\alpha(R(t))\rangle$, and 0 for all the other states.

To characterize the photoinduced charge transfer dynamics in a given system, we compute the time-dependent charge populations on each moiety (such as a donor or acceptor) of the system. The charge population on a specific fragment is obtained by projecting the adiabatic reduced density matrix onto the atomic orbital (AO) basis associated with that molecular moiety $\mathcal{N}$ as follows[10,11]

$$P_{\mathcal{N}}(t) = \text{Re}\left[\sum_{\mu \in \mathcal{N}}^\nu \sum_{ij} \rho_{ij}(t) C_{\mu i}(\mathbf{R}(t)) S_{\mu\nu} C_{\nu j}(\mathbf{R}(t)) \right] \tag{14}$$

where $S_{\mu\nu} = \langle \varphi_\mu(\mathbf{r}, \mathbf{R}(t)) | \varphi_\nu(\mathbf{r}, \mathbf{R}(t)) \rangle$ is the AO overlap matrix, and $\{C_{\mu i}(\mathbf{R}(t))\}$ are the AO expansion coefficients obtained by solving eq 3 in the AO basis (through the self-consistent procedure[55]) as follows

$$|\phi_i(\mathbf{R}(t))\rangle = \sum_\mu C_{\mu i}(\mathbf{R}(t)) |\varphi_\mu(\mathbf{r}, \mathbf{R})\rangle \tag{15}$$

Note that in eq 14, we choose to use the active state estimator (eq 12) for the adiabatic electronic population and the electronic estimator (eq 13) for the adiabatic electronic coherence. This choice has shown to provide the most accurate diabatic population.[54] The expectation value of the charge population is obtained as

$$\bar{P}_{\mathcal{N}}(t) = \langle P_{\mathcal{N}}(t) \rangle \tag{16}$$

where $\langle \cdots \rangle$ represents the ensemble average over the CPA-FSSH trajectories, and $P_{\mathcal{N}}(t)$ is the charge population estimator expressed in eq 14.

■ COMPUTATIONAL DETAILS

All electronic structure calculations are performed using the semiempirical Density Functional Tight-Binding (DFTB) method,[55−57] which is an approximation to the KS-DFT. Earlier works have demonstrated that DFTB provides accurate electronic structure for studying charge transfer dynamics in various organophotovoltaic complexes.[38,58,59] More specifically, DFTB3 method,[57] which is a third-order Taylor expansion of the DFT total energy around a reference density, is used in this work. DFTB3 is proven to be a well-suited method[57] to describe the charges in systems with C, H, N, O, and P elements, with improved Coulomb interaction between atomic partial charges.[57] Electronic structure calculations in this work are performed with the DFTB3 method and the 3ob-3-1 Slater−Koster parameter set[60] as implemented in the 17.1 version of the DFTB+ package.[61] We also included the dispersion interactions using the Lennard-Jones dispersion model with the UFF parameters[62] as implemented in the DFTB+ code.

The initial nuclear geometries are obtained according to the ground state canonical ensemble, through the following procedure. First, the system is equilibrated in the NVT ensemble for 100 ps with a nuclear time-step dt = 0.5 fs, using the Nosé−Hoover chain thermostat as implemented in the DFTB+ package. From this NVT trajectory, we collected 50 different initial conditions (coordinates and velocities at every 2 ps interval) for the subsequent nonadiabatic dynamics propagation.

The initial electronic excitation $|\Psi(\mathbf{r}, 0)\rangle$ is modeled as the LUMO of the donor moiety $|\phi_{\text{LUMO}}^D\rangle$, which is a widely used approximation for simulating photoinduced charge transfer dynamics.[10,11] This choice provides a reasonable single-electron picture of the localized photoexcitation in the system. Here, the LUMO of the donor moiety is obtained from a separate DFTB3 calculation performed for the isolated donor moiety.[10,11,37,63] The initial coefficients for the electronic states are computed as $c_i(0) = \langle \phi_i(\mathbf{R}(0) | \phi_{\text{LUMO}}^D \rangle = \sum_\mu C_{\mu i}(\mathbf{R}(0)) \langle \varphi_\mu(\mathbf{R}(0)) | \sum_\nu C_\nu^D(\mathbf{R}(0)) | \varphi_\nu(\mathbf{R}(0)) \rangle = \sum_{\mu\nu} C_{\mu i}(\mathbf{R}(0)) S_{\mu\nu}(\mathbf{R}(0)) C_\nu^D(\mathbf{R}(0))$, which is evaluated with zero expansion coefficients over the AOs on the acceptor moiety. The active state at $t = 0$ in the CPA-FSSH calculation is chosen stochastically among $|\phi_i(\mathbf{R}(0))\rangle$ based upon the probability of $|c_i(0)|^2$.

For the CPA-FSSH nonadiabatic dynamics simulations, the nuclear propagation is performed using the velocity-Verlet integrator with a time-step of dt = 0.1 fs under the NVE ensemble. Adapting the classical path approximation (CPA),[9−11,41] we used the ground state DFTB3 gradients (cf. eq 4) during the nuclear propagation. To obtain the time-dependent electronic expansion coefficients, we numerically integrated eq 7 using the fourth-order Runge−Kutta algorithm with a time-step of dt = 10^{-3} fs. To compute the time-dependent nonadiabatic couplings, we adapted a well-established finite difference approximation[64] as follows

$$\langle \phi_j | \frac{\partial}{\partial t} \phi_i \rangle = \frac{1}{2\tau} [\langle \phi_j(t) | \phi_i(t+\tau) \rangle - \langle \phi_j(t+\tau) | \phi_i(t) \rangle]$$

(17)

where the MO overlaps $\langle \phi_j(t+\tau) | \phi_i(t) \rangle$ at different time-steps needs to be carefully calculated by following the random phases of the MOs generated from the electronic structure calculations.[65−67] By expanding the MOs as linear combinations of the atomic orbitals (AOs), i.e., $|\phi_i(\mathbf{R}(t))\rangle = \sum_\mu C_{\mu i}(\mathbf{R}(t))|\varphi_\mu(\mathbf{R})\rangle$, the overlap between two MOs in eq 17 can be computed as

$$\langle \phi_j(\mathbf{R}(t+\tau)) | \phi_i(\mathbf{R}(t)) \rangle$$
$$= \sum_{\mu\nu} C_{\mu j}(\mathbf{R}(t+\tau)) C_{\nu i}(\mathbf{R}(t)) S_{\mu\nu}(t+\tau, t),$$

(18)

where, $S_{\mu\nu}(t+\tau, t)$ is the overlap between two atomic orbitals (AOs) at two different time-steps

$$S_{\mu\nu}(t+\tau, t) = \langle \varphi_\mu(\mathbf{r}, \mathbf{R}(t+\tau)) | \varphi_\nu(\mathbf{r}, \mathbf{R}(t)) \rangle$$

(19)

These AO overlap integrals are explicitly evaluated with our in-house version of DFTB+ code.

A total of 50 initial nuclear configurations are used for the ensemble average, and for each nuclear configuration, a total of 10^4 CPA-FSSH trajectories are used. Expectation values are calculated through the ensemble average over specific CPA-FSSH trajectories on top of each nuclear trajectory.

Figure 1 depicts the optimized geometries of the model system considered in this work: (A) $2H_2Pc/C_{60}$ (B) $2H_2Pc/C_{70}$,
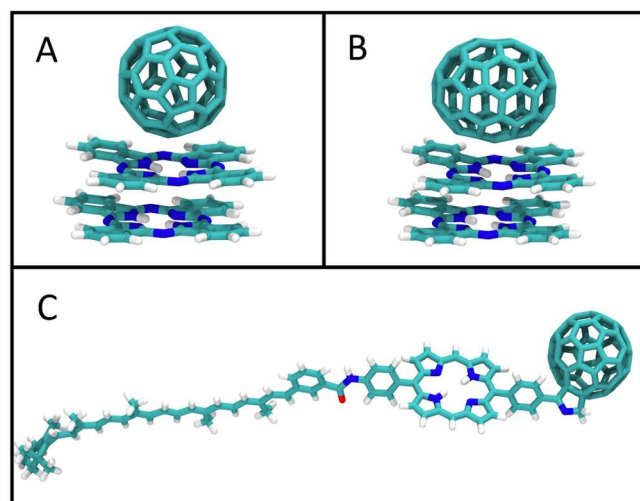
Figure 1. Structures of the model systems investigated in this paper: (A) $2H_2Pc/C_{60}$ (B) $2H_2Pc/C_{70}$ and (C) carotenoid−porphyrin−C_{60}(CPC) triad. All geometries presented in this figure are optimized at the DFTB3 level of theory.

and (C) carotenoid−porphyrin−fullerene (CPC_{60}) triad. The Cartesian coordinates of the optimized nuclear geometries (at the level of DFTB3) are provided in the Supporting Information. For the $2H_2Pc/C_{60}$ and $2H_2Pc/C_{70}$ model systems, we considered H_2Pc dimer as the donor,[12] and for the CPC triad, porphyrin is considered as the donor moiety.[37] To reduce the computational cost, we only consider a finite size of CPA-FSSH active space that includes the LUMO to LUMO+9 orbitals of the entire system, which are the low-lying orbitals that participate directly in the photoinduced charge transfer process.

We carefully checked that the nonadiabatic dynamics is confined within this subspace, i.e., further increasing the active space does not influence the dynamics.[68]

■ RESULTS AND DISCUSSIONS

Figure 2 presents the time dependent nonadiabatic dynamics of the $2H_2Pc/C_{60}$ system with a specific nuclear trajectory through

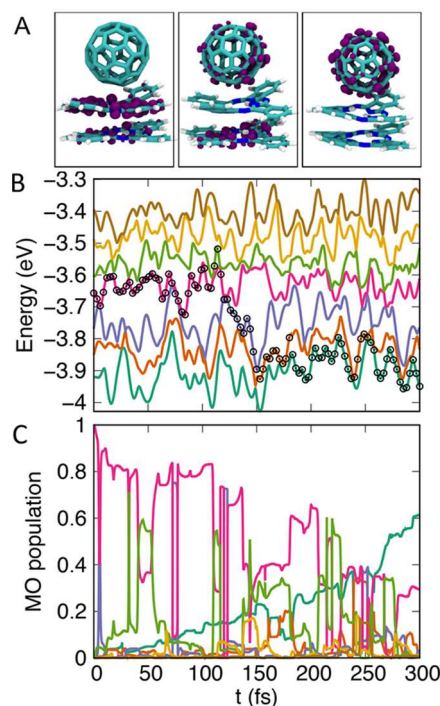**Figure 2.** (A) Charge density of the active state along a given nuclear trajectory of the phthalocyanine dimer/fullerene ($2H_2Pc/C_{60}$) system, at $t = 32.2$ fs, $t = 119.6$ fs, and $t = 150$ fs, respectively. (B) Time-dependent energies of $|\phi_i(\mathbf{R}(t))\rangle$ (LUMO to LUMO+6) along a give nuclear trajectory. The time-dependent active states for a given CPA-FSSH trajectory are indicated with black open circles. (C) The adiabatic (MO) populations (eq 11) for the same nuclear trajectory, averaged over 10,000 CAP-FSSH trajectories (with the corresponding color coding of the MOs in panel B for LUMO to LUMO+6.)

the CPA-FSSH simulation. Figure 2A depicts the transferring charge density of the active state along a given nuclear trajectory at $t = 32.2$ fs, $t = 119.6$ fs, and $t = 150$ fs, respectively. The initial charge density is sensitive to the nuclear geometries, which can either localize on one of the H_2Pc molecules, or delocalize over the H_2Pc dimer. An additional analysis is provided in the Supporting Information. Figure 2B presents the time-dependent orbital energies of $|\phi_i(\mathbf{R}(t))\rangle$(LUMO to LUMO+6) of this system. As shown in the figure, the MO orbital energies come close to each other at various instances of time, forming avoided crossings where the nonadiabatic coupling element between the surfaces would be large and resulting in a higher probability for the active state to hop from one surface to the other (see eq 8). The character of the activate state changes due to both the motion of the nuclei (from the first to the second panel in Figure 2A) as well as nonadiabatic transitions among states (from the second to the third panel in Figure 2A). The former and the latter ways are classified as the adiabatic vs nonadiabatic contribution of the charge transfer.[69] Figure 2C presents the time-dependent MO electronic population of the $2H_2Pc/C_{60}$ system along one specific nuclear trajectory, computed through

the ensemble average of 10^4 CPA-FSSH trajectories through eq 11, color coded according to the MOs presented in Figure 2B. The nonadiabatic transitions occur at the avoid crossings in Figure 2B.

Figure 3 presents the population dynamics obtained over an ensemble average of 50 nuclear trajectories with 10^4 CPA-FSSH
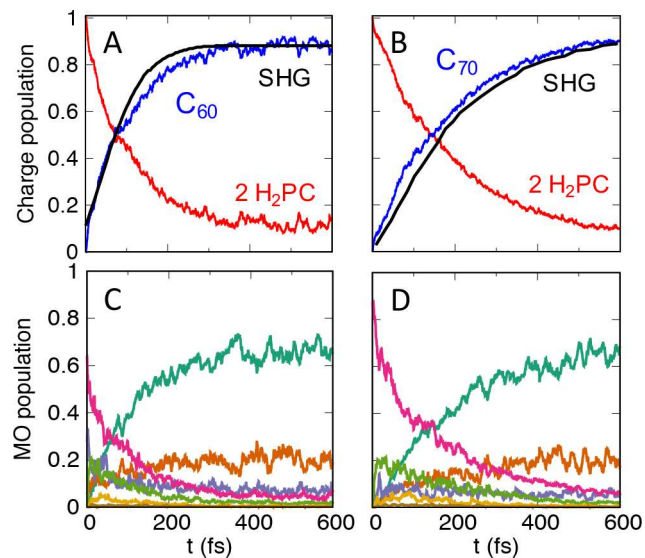

Figure 3. (A) Charge population on C_{60} (blue), on $2H_2Pc$ (red), as well as the SHG experimental signal (black) adapted from ref 12 that indicate the time-dependent charge density on C_{60}. (B) Time-dependent charge population of the $2H_2Pc/C_{70}$ system. (C and D) presents the MO populations of $2H_2Pc/C_{60}$ and $2H_2Pc/C_{70}$, respectively, with the color coding corresponds to the energy levels in Figure 2b.

trajectories on top of each nuclear trajectory. Figure 3A presents the charge population $P_N(t)$ (eq 14) of the donor molecules $2H_2Pc$ (red) and the acceptor molecule C_{60} (blue) in the $2H_2Pc/C_{60}$ system. To assess the accuracy of our direct simulations, the experimentally measured time-dependent charge population on fullerene, which is based on transient second harmonic generation (SHG) spectroscopy,[12] is presented (black curve). Our theoretical results almost quantitatively reproduce the experimental measurements, as

well as FSSH simulation using configuration-interaction Singles-Doubles (CISD) with the Pariser–Parr–Pople (PPP) level of theory,[12] suggesting a reasonable accuracy and reliability of the current simulation approach. On the other hand, due to the large number of approximations made in our current theoretical approach (including the propagation of nuclei on the ground electronic state, the single-particle treatment, and the ignorance of decoherence corrections in the FSSH approach), it is also possible that a significant error cancellations leads to accurate results in the end.

Figure 3B presents the charge population of the donor molecules $2H_2Pc$ (red) and the acceptor molecule C_{70} (blue) in the $2H_2Pc/C_{70}$ system. This simulation successfully predicts a slower charge transfer dynamics in $2H_2Pc/C_{70}$ system compared to $2H_2Pc/C_{60}$, as observed in the SHG experiments. Figure 3C–D presents the corresponding MO population (computed from eq 11) associated with $2H_2Pc/C_{60}$ and $2H_2Pc/C_{70}$, respectively, with the same color coding for the MO orbitals used for LUMO to LUMO+6 in Figure 2B.

Figure 4 presents the CT dynamics in the CPC triad model system, which is another well-studied prototypical artificial light-harvesting system.[13,19,37,39] Earlier experimental investigations[70,71] have shown photoinduced charge separation in this system. Recent theoretical work suggests that the simple Marcus theory is unable to properly predict the photoinduced electron-transfer time-scales in this system.[13,39] Here, we use direct nonadiabatic simulations to investigate the charge transfer dynamics. Figure 4A, presents the time-dependent transferring charge density of the corresponding active state along a given nuclear trajectory at $t = 0$ fs, $t = 94.2$ fs, and $t = 600$ fs, respectively. Figure 4B presents the time-dependent orbital energies of $|\phi_i(R(t))\rangle$(LUMO to LUMO+6) of this system. Figure 4C presents the corresponding electronic populations of each MO (based on eq 11), and Figure 4D presents the charge population (based on eq 14) for the PPH (blue), CAR (green), and the C_{60} (red) moiety. The population dynamics is obtained from the ensemble average of 10^4 CPA-FSSH trajectories per nuclear trajectory, and 50 nuclear trajectories in total.

Our simulations suggest a significant amount (90%) of charge transfer from the porphyrin moiety to the C_{60} occurring within ∼0.4 ps time-scale, and a complete charge transfer to the C_{60} moiety within ∼0.6 ps time-scale. Earlier theoretical works in related systems (with a few functional groups on the porphyrin
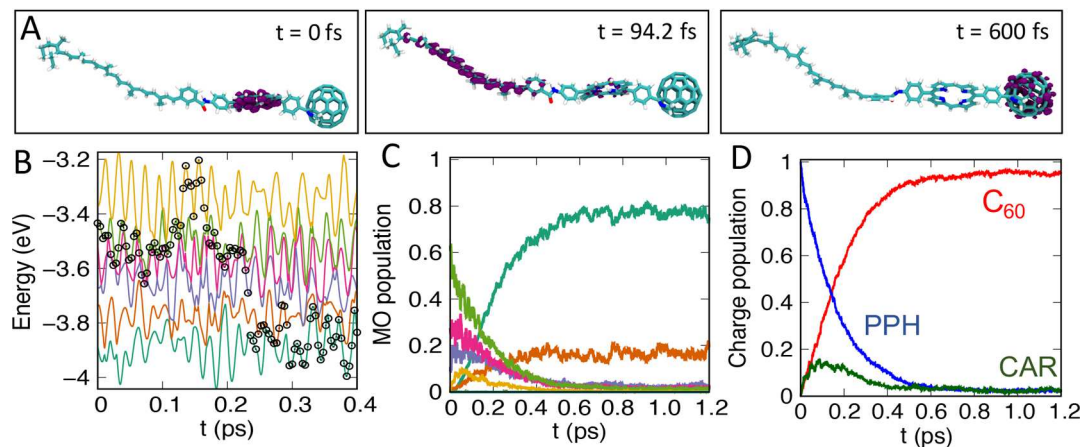

Figure 4. Photoinduced charge transfer dynamics of the CPC triad. (A) Charge density of the active state MO at time t. (B) Time-dependent MO energies and the active states (black open circles), (C) MO populations, and (D) time-dependent charge population on each moiety.

and the fullerene moieties) show that the predicted CT time scales are spanned over a range of 70 fs[19] (when completely ignore the motion of nuclei) to 3−5 ps.[13,37,38] In a combined experimental and computational study, it has shown that the formation of $[C-P]^+-C_{60}^-$ is within 70 fs.[19] On the other hand, for the synthesized CPC triad, the formation of the CT state is within 10 ps.[70] Recent work based on the linearized semiclassical nonequilibrium Fermi's Golden Rule (as well as the instantaneous Marcus theory)[39] suggest that 90% of the CT occurs during the first 0.6 ps of the simulation for the bent configuration of CTC, agreeing with what we find from our direct simulation. Together, all the above results clearly demonstrate that the current direct simulation approach is both efficient and accurate to investigate the photoinduced charge transfer dynamics.

CONCLUSIONS

This work presents the direct nonadiabatic simulation of photoinduced charge transfer reaction in well-studied phthalocyanine/fullerene and carotenoid-porphyrin-fullerene systems. We demonstrate that our approach can predict the time scales of CT dynamics that are in well-agreement with both experimental results[12] and theoretical studies.[12,39] Due to the computationally inexpensive nature of the time-dependent DFT with the semiempirical DFTB calculations, the DFTB-CPA-FSSH approach shows promise for investigating the CT dynamics in large systems.

Despite the success of the current approach in simulating the model systems presented in this work, we acknowledge its potential limitations, including (i) the single-particle picture that could fail for the strongly coupled electron and hole dynamics,[22,36,37,41,72] (ii) the validity of the classical path approximation,[47,53,63,73] and (iii) the accuracy of the FSSH algorithms.[43,52] Encouraging progress is being made to address each of the above three challenges, enabling the possibility to obtain a more accurate description of the charge transfer dynamics in large complex systems.

ASSOCIATED CONTENT

Ⓢ Supporting Information

The Supporting Information is available free of charge at https://pubs.acs.org/doi/10.1021/acs.jpca.0c10151.

Figures showing the adiabatic and charge populations and charge density on each molecule at the first frame of the NAMD simulation, Cartesian coordinates of the optimized nuclear geometries for systems considered in this work (PDF)

AUTHOR INFORMATION

Corresponding Authors

Sharma S. R. K. C. Yamijala − *Department of Chemistry, University of Rochester, Rochester, New York 14627, United States; Department of Chemistry, Indian Institute of Technology-Madras, Chennai 600036, India;* ⓞ orcid.org/0000-0003-1773-9226; Email: yamijala@iitm.ac.in

Pengfei Huo − *Department of Chemistry, University of Rochester, Rochester, New York 14627, United States;* ⓞ orcid.org/0000-0002-8639-9299; Email: pengfei.huo@rochester.edu

Complete contact information is available at:
https://pubs.acs.org/10.1021/acs.jpca.0c10151

Notes
The authors declare no competing financial interest.

REFERENCES

(1) Marcus, R. A. Electrostatic free energy and other properties of states having nonequilibrium polarization. I. *J. Chem. Phys.* **1956**, *24*, 979−989.

(2) Marcus, R. A. On the theory of oxidation-reduction reactions involving electron transfer. I. *J. Chem. Phys.* **1956**, *24*, 966−978.

(3) Wörner, H. J.; et al. Charge migration and charge transfer in molecular systems. *Struct. Dyn.* **2017**, *4*, 061508.

(4) May, V.; Kühn, O. *Charge and energy transfer dynamics in molecular systems*; John Wiley & Sons: 2008.

(5) Blankenship, R. E. *Molecular mechanisms of photosynthesis*; John Wiley & Sons: 2014.

(6) Barber, J.; Tran, P. D. From natural to artificial photosynthesis. *J. R. Soc., Interface* **2013**, *10*, 20120984.

(7) Rivalta, I.; Brudvig, G. W.; Batista, V. S. Oxomanganese complexes for natural and artificial photosynthesis. *Curr. Opin. Chem. Biol.* **2012**, *16*, 11−18.

(8) Duncan, W. R.; Prezhdo, O. V. Theoretical studies of photoinduced electron transfer in dye-sensitized TiO2. *Annu. Rev. Phys. Chem.* **2007**, *58*, 143−184.

(9) Duncan, W. R.; Craig, C. F.; Prezhdo, O. V. Time-Domain ab Initio Study of Charge Relaxation and Recombination in Dye-Sensitized TiO2. *J. Am. Chem. Soc.* **2007**, *129*, 8528−8543.

(10) Rego, L. G.; Batista, V. S. Quantum Dynamics Simulations of Interfacial Electron Transfer in Sensitized TiO2 Semiconductors. *J. Am. Chem. Soc.* **2003**, *125*, 7989−7997.

(11) Abuabara, S. G.; Rego, L. G. C.; Batista, V. S. Influence of Thermal Fluctuations on Interfacial Electron Transfer in Functionalized TiO2 Semiconductors. *J. Am. Chem. Soc.* **2005**, *127*, 18234−18242.

(12) Jailaubekov, A. E.; Willard, A. P.; Tritsch, J. R.; Chan, W.-L.; Sai, N.; Gearba, R.; Kaake, L. G.; Williams, K. J.; Leung, K.; Rossky, P. J.; Zhu, X.-Y. Hot Charge-Transfer Excitons Set the Time Limit for Charge Separation at Donor/Acceptor Interfaces in Organic Photovoltaics. *Nat. Mater.* **2013**, *12*, 66−73.

(13) Sun, X.; Zhang, P.; Lai, Y.; Williams, K. L.; Cheung, M. S.; Dunietz, B. D.; Geva, E. Computational Study of Charge-Transfer Dynamics in the Carotenoid-Porphyrin-C60 Molecular Triad Solvated in Explicit Tetrahydrofuran and Its Spectroscopic Signature. *J. Phys. Chem. C* **2018**, *122*, 11288−11299.

(14) Coropceanu, V.; Chen, X.-K.; Wang, T.; Zheng, Z.; Brédas, J.-L. Charge-transfer electronic states in organic solar cells. *Nat. Rev. Mater.* **2019**, *4*, 689−707.

(15) Akimov, A. V.; Neukirch, A. J.; Prezhdo, O. V. Theoretical insights into photoinduced charge transfer and catalysis at oxide interfaces. *Chem. Rev.* **2013**, *113*, 4496−4565.

(16) Torres, A.; Oliboni, R. S.; Rego, L. G. Vibronic and Coherent Effects on Interfacial Electron Transfer Dynamics. *J. Phys. Chem. Lett.* **2015**, *6*, 4927−4935.

(17) Mukherjee, S.; Bowman, D. N.; Jakubikova, E. Cyclometalated Fe(II) Complexes as Sensitizers in Dye-Sensitized Solar Cells. *Inorg. Chem.* **2015**, *54*, 560−569.

(18) Lee, M.; Geva, E.; Dunietz, B. Donor-to-Donor vs. Donor-to-Acceptor Interfacial Charge Transfer States in the Phthalocyanine-Fullerene Organic Photovoltaic System. *J. Phys. Chem. Lett.* **2014**, *5*, 3810−3816.

(19) Rozzi, C. A.; Falke, S. M.; Spallanzani, N.; Rubio, A.; Molinari, E.; Brida, D.; Maiuri, M.; Cerullo, G.; Schramm, H.; Christoffers, J.; Lienau, C. Quantum coherence controls the charge separation in a prototypical artificial light-harvesting system. *Nat. Commun.* **2013**, *4*, 1602.

(20) Tamura, H.; Burghardt, I. Ultrafast Charge Separation in Organic Photovoltaics Enhanced by Charge Delocalization and Vibronically Hot Exciton Dissociation. *J. Am. Chem. Soc.* **2013**, *135*, 16364−16367.

(21) Huix-Rotllant, M.; Tamura, H.; Burghardt, I. Concurrent Effects of Delocalization and Internal Conversion Tune Charge Separation at Regioregular PolythiopheneFullerene Heterojunctions. *J. Phys. Chem. Lett.* **2015**, *6*, 1702−170.

(22) Patel, K.; Bittner, E. R. Mixed Quantum Classical Simulations of Charge-Transfer Dynamics in a Model Light-Harvesting Complex. I. Charge-Transfer Dynamics. *J. Phys. Chem. B* **2020**, *124*, 2149−2157.

(23) Patel, K.; Bittner, E. R. Mixed Quantum Classical Simulations of Charge-Transfer Dynamics in a Model Light-Harvesting Complex. II. Transient Vibrational Analysis. *J. Phys. Chem. B* **2020**, *124*, 2158−2167.

(24) Giannini, S.; Carof, A.; Ellis, M.; Yang, H.; Ziogos, O. G.; Ghosh, S.; Blumberger, J. Quantum localization and delocalization of charge carriers in organic semiconducting crystals. *Nat. Commun.* **2019**, *10*, 3843.

(25) Carof, A.; Giannini, S.; Blumberger, J. How to calculate charge mobility in molecular materials from surface hopping non-adiabatic molecular dynamics − beyond the hopping/band paradigm. *Phys. Chem. Chem. Phys.* **2019**, *21*, 26368.

(26) Zhu, H.; Yang, Y.; Hyeon-Deuk, K.; Califano, M.; Song, N.; Wang, Y.; Zhang, W.; Prezhdo, O.; Lian, T. Auger-Assisted Electron Transfer from Photoexcited Semiconductor Quantum Dots. *Nano Lett.* **2014**, *14*, 1263−1269.

(27) Hyeon-Deuk, K.; Kim, J.; Prezhdo, O. V. Ab Initio Analysis of Auger-Assisted Electron Transfer. *J. Phys. Chem. Lett.* **2015**, *6*, 244−249.

(28) Trivedi, D.; Wang, L.; Prezhdo, O. Auger-mediated electron relaxation is robust to deep hole traps: time-domain ab initio study of CdSe quantum dots. *Nano Lett.* **2015**, *15*, 2086−2091.

(29) Goyal, P.; Hammes-Schiffer, S. Role of Solvent Dynamics in Photoinduced Proton-Coupled Electron Transfer in Phenol-Amine Complex in Solution. *J. Phys. Chem. Lett.* **2015**, *6*, 3515−3520.

(30) Goyal, P.; Schwerdtfeger, C. A.; Soudackov, A. V.; Hammes-Schiffer, S. Proton Quantization and Vibrational Relaxation in Nonadiabatic Dynamics of Photoinduced Proton-Coupled Electron Transfer in a Solvated Phenol-Amine Complex. *J. Phys. Chem. B* **2016**, *120*, 2407−2417.

(31) Goyal, P.; Hammes-Schiffer, S. Tuning the Ultrafast Dynamics of Photoinduced Proton-Coupled Electron Transfer in Energy Conversion Processes. *ACS Energy Lett.* **2017**, *2*, 512−519.

(32) Wang, L.; Long, R.; Prezhdo, O. V. Time-Domain Ab Initio Modeling of Photoinduced Dynamics at Nanoscale Interfaces. *Annu. Rev. Phys. Chem.* **2015**, *66*, 549−579.

(33) Tully, J. C. Molecular dynamics with Electronic Transitions. *J. Chem. Phys.* **1990**, *93*, 1061−1071.

(34) Pal, S.; Trivedi, D. J.; Akimov, A. V.; Aradi, B.; Frauenheim, T.; Prezhdo, O. V. Nonadiabatic molecular dynamics for thousand atom systems: A tight-binding approach toward pyxaid. *J. Chem. Theory Comput.* **2016**, *12*, 1436−1448.

(35) Fischer, S. A.; Habenicht, B. F.; Madrid, A. B.; Duncan, W. R.; Prezhdo, O. V. Regarding the validity of the time-dependent Kohn−Sham approach for electron-nuclear dynamics via trajectory surface hopping. *J. Chem. Phys.* **2011**, *134*, 024102.

(36) Liu, X.-Y.; Li, Z.-W.; Fang, W.-H.; Cui, G. Nonadiabatic Exciton and Charge Separation Dynamics at Interfaces of Zinc Phthalocyanine and Fullerene: Orientation Does Matter. *J. Phys. Chem. A* **2020**, *124*, 7388−7398.

(37) Rego, L. G.; Hames, B. C.; Mazon, K. T.; Joswig, J.-O. Intramolecular polarization induces electron−hole charge separation in light-harvesting molecular triads. *J. Phys. Chem. C* **2014**, *118*, 126−134.

(38) High, J. S.; Rego, L. G.; Jakubikova, E. Quantum dynamics simulations of excited state energy transfer in a zinc−free-base porphyrin dyad. *J. Phys. Chem. A* **2016**, *120*, 8075−8084.

(39) Hu, Z.; Tong, Z.; Cheung, M. S.; Dunietz, B. D.; Geva, E.; Sun, X. Photoinduced Charge Transfer Dynamics in the Carotenoid-Porphyrin-C60 Triad via the Linearized Semiclassical Nonequilibrium Fermi's Golden Rule. *J. Phys. Chem. B* **2020**, *124*, 9579−9591.

(40) Koch, W.; Holthausen, M. C. *A Chemist's Guide to Density Functional Theory*; John Wiley & Sons: 2001.

(41) Akimov, A. V.; Prezhdo, O. V. The PYXAID Program for Non-Adiabatic Molecular Dynamics in Condensed Matter Systems. *J. Chem. Theory Comput.* **2013**, *9*, 4959−4972.

(42) Akimov, A.; Prezhdo, O. *Theory of Nonadiabatic Electron Dynamics in Nanomaterials*; 2015.

(43) Wang, L.; Akimov, A.; Prezhdo, O. V. Recent Progress in Surface Hopping: 2011−2015. *J. Phys. Chem. Lett.* **2016**, *7*, 2100−2112.

(44) Doltsinis, N. L.; Marx, D. First principles molecular dynamics involving excited states and nonadiabatic transitions. *J. Theor. Comput. Chem.* **2002**, *01*, 319−349.

(45) Akimov, A. V.; Prezhdo, O. V. Advanced capabilities of the PYXAID program: integration schemes, decoherence effects, multi-excitonic states, and field-matter interaction. *J. Chem. Theory Comput.* **2014**, *10*, 789−804.

(46) Craig, C. F.; Duncan, W. R.; Prezhdo, O. V. Trajectory surface hopping in the time-dependent Kohn-Sham approach for electron-nuclear dynamics. *Phys. Rev. Lett.* **2005**, *95*, 163001.

(47) Gao, X.; Geng, H.; Peng, Q.; Ren, J.; Yi, Y.; Wang, D.; Shuai, Z. Nonadiabatic Molecular Dynamics Modeling of the Intrachain Charge Transport in Conjugated Diketopyrrolo-Pyrrole Polymers. *J. Phys. Chem. C* **2014**, *118*, 6631−6640.

(48) Akimov, A. V. Nonadiabatic Molecular Dynamics with Tight-Binding Fragment Molecular Orbitals. *J. Chem. Theory Comput.* **2016**, *12*, 5719−5736.

(49) High, J. S.; Rego, L. G. C.; Jakubikova, E. Quantum Dynamics Simulations of Excited State Energy Transfer in a Zinc−Free-Base Porphyrin Dyad. *J. Phys. Chem. A* **2016**, *120*, 8075−8084.

(50) Humeniuk, A.; Mitric, R. *DFTBaby: A Software Package for Non-Adiabatic Molecular Dynamics Simulations Based on Long-Range Corrected Tight-Binding TD-DFT(B)*; 2017.

(51) Parandekar, P. V.; Tully, J. C. Detailed balance in Ehrenfest mixed quantum-classical dynamics. *J. Chem. Theory Comput.* **2006**, *2*, 229−235.

(52) Subotnik, J. E.; Jain, A.; Landry, B.; Petit, A.; Ouyang, W.; Bellonzi, N. Understanding the Surface Hopping View of Electronic Transitions and Decoherence. *Annu. Rev. Phys. Chem.* **2016**, *67*, 387−417.

(53) Smith, B.; Akimov, A. V. A comparative analysis of surface hopping acceptance and decoherence algorithms within the neglect of back-reaction approximation. *J. Chem. Phys.* **2019**, *151*, 124107.

(54) Landry, B. R.; Falk, M. J.; Subotnik, J. E. Communication: The correct interpretation of surface hopping trajectories: How to calculate electronic properties. *J. Chem. Phys.* **2013**, *139*, 211101.

(55) Elstner, M.; Porezag, D.; Jungnickel, G.; Elsner, J.; Haugk, M.; Frauenheim, T.; Suhai, S.; Seifert, G. Self-consistent-charge density-functional tight-binding method for simulations of complex materials properties. *Phys. Rev. B: Condens. Matter Mater. Phys.* **1998**, *58*, 7260.

(56) Porezag, D.; Frauenheim, T.; Köhler, T.; Seifert, G.; Kaschner, R. Construction of tight-binding-like potentials on the basis of density-functional theory: Application to carbon. *Phys. Rev. B: Condens. Matter Mater. Phys.* **1995**, *51*, 12947.

(57) Gaus, M.; Cui, Q.; Elstner, M. DFTB3: Extension of the Self-Consistent-Charge Density-Functional Tight-Binding Method (SCC-DFTB). *J. Chem. Theory Comput.* **2011**, *7*, 931−948.

(58) Scholz, R.; Luschtinetz, R.; Seifert, G.; Jägeler-Hoheisel, T.; Körner, C.; Leo, K.; Rapacioli, M. Quantifying charge transfer energies at donor−acceptor interfaces in small-molecule solar cells with

constrained DFTB and spectroscopic methods. *J. Phys.: Condens. Matter* **2013**, *25*, 473201.

(59) Oviedo, M. B.; Wong, B. M. Real-time quantum dynamics reveals complex, many-body interactions in solvated nanodroplets. *J. Chem. Theory Comput.* **2016**, *12*, 1862−1871.

(60) Gaus, M.; Goez, A.; Elstner, M. Parametrization and Benchmark of DFTB3 for Organic Molecules. *J. Chem. Theory Comput.* **2013**, *9*, 338−354.

(61) Aradi, B.; Hourahine, B.; Frauenheim, T. DFTB+, a Sparse Matrix-Based Implementation of the DFTB Method. *J. Phys. Chem. A* **2007**, *111*, 5678−5684.

(62) Rappe, A. K.; Casewit, C. J.; Colwell, K. S.; Goddard, W. A.; Skiff, W. M. UFF, a Full Periodic Table Force Field for Molecular Mechanics and Molecular Dynamics Simulations. *J. Am. Chem. Soc.* **1992**, *114*, 10024−10035.

(63) Torres, A.; Oliboni, R. S.; Rego, L. G. Vibronic and Coherent Effects on Interfacial Electron Transfer Dynamics. *J. Phys. Chem. Lett.* **2015**, *6*, 4927−4935.

(64) Hammes-Schiffer, S.; Tully, J. C. Proton Transfer in Solution: Molecular Dynamics with Quantum Transitions. *J. Chem. Phys.* **1994**, *101*, 4657−4667.

(65) Space, B.; Coker, D. Nonadiabatic Dynamics of Excited Excess Electrons in Simple Fluids. *J. Chem. Phys.* **1991**, *94*, 1976−1984.

(66) Yu, N.; Margulis, C.; Coker, D. Influence of Solvation Environment on Excited State Avoided Crossings and Photo-dissociation Dynamics. *J. Phys. Chem. B* **2001**, *105*, 6728−6737.

(67) Hu, C.; Sugino, O.; Hirai, H.; Tateyama, Y. Nonadiabatic couplings from the Kohn-Sham derivative matrix: Formulation by time-dependent density-functional theory and evaluation in the pseudopotential framework. *Phys. Rev. A: At., Mol., Opt. Phys.* **2010**, *82*, 062508.

(68) Mandal, A.; Yamijala, S. S.; Huo, P. Quasi-Diabatic Representation for Nonadiabatic Dynamics Propagation. *J. Chem. Theory Comput.* **2018**, *14*, 1828−1840.

(69) Long, R.; English, N. J.; Prezhdo, O. V. Photo-induced Charge Separation across the GrapheneTiO2 Interface Is Faster than Energy Losses: A Time-Domain ab Initio Analysis. *J. Am. Chem. Soc.* **2012**, *134*, 14238−14248.

(70) Liddell, P. A.; Kuciauskas, D.; Sumida, J. P.; Nash, B.; Nguyen, D.; Moore, A. L.; Moore, T. A.; Gust, D. Photoinduced charge separation and charge recombination to a triplet state in a carotene-porphyrin- fullerene triad. *J. Am. Chem. Soc.* **1997**, *119*, 1400−1405.

(71) Gust, D.; Moore, T. A.; Moore, A. L. Mimicking photosynthetic solar energy transduction. *Acc. Chem. Res.* **2001**, *34*, 40−48.

(72) da Silva Oliboni, R.; Bortolini, G.; Torres, A.; Rego, L. G. C. A Nonadiabatic Excited State Molecular Mechanics/Extended Hückel Ehrenfest Method. *J. Phys. Chem. C* **2016**, *120*, 27688−27698.

(73) Nijjar, P.; Jankowska, J.; Prezhdo, O. V. Ehrenfest and classical path dynamics with decoherence and detailed balance. *J. Chem. Phys.* **2019**, *150*, 204124.